Journal of Zhejiang University SCIENCE
ISSN 1009-3095
http://www.zju.edu.cn/jzus
E-mail: jzus@zju.edu.cn

Three-dimensional transient numerical simulation for gas exchange process in a four-stroke motorcycle engine

WANG Chun-fa (王春发)†, CHEN Guo-hua (陈国华), LUO Ma-ji (罗马吉), YANG Wan-li (杨万里)

(*School of Energy and Power Engineering, Huazhong University of Science and Technology, Wuhan 430074, China*)

†E-mail: hustwang@163.com

Received Apr. 8, 2005; revision accepted Aug. 3, 2005

Abstract: Three-dimensional transient numerical simulation of gas exchange process in a four-stroke motorcycle engine with a semi-spherical combustion chamber with two tilt valves was studied. Combination of the grid re-meshing method and the snapper technique made the valves move smoothly. The flow structure and pattern in a complete engine cycle were described in detail. Tumble ratios around the *x*-axis and *y*-axis were analyzed. Comparison of computed pressure with experimental pressure under motored condition revealed that the simulation had high calculation precision; CFD simulation can be regarded as an important tool for resolving the complex aerodynamic behavior in motorcycle engines.

Key words: Motorcycle engine, Gas exchange process, Transient numerical simulation, Dynamic grid generation
doi:10.1631/jzus.2005.A1137 **Document code:** A **CLC number:** TK411.3

INTRODUCTION

In-cylinder flow characteristics during fuel injection and subsequent interactions with fuel sprays and combustion are important effect on engine performance and exhaust emissions of an engine (Floch *et al*., 1998; Kim *et al*., 1999). Four key parameters control the flow field in an engine: the mean flow components, the stability of the mean flow, the temporal turbulence evolution during the intake and compression strokes, and the mean velocity near the spark gap at the time of ignition (Zhao *et al*., 1999). Experiment and 3-D numerical simulation are two methods for researching the flow characteristics in an engine. In comparison with experiment, 3-D numerical simulation involves minimal money and time and has become a more and more commonly used tool for new engine design.

To meet increasingly stringent emission requirements, 3-D numerical simulation of the engine full cycle process is very important (Gosam, 1999; Johan *et al*., 2001). A four-stroke motorcycle engine's structure is complex and compact, and its 3-D simulation is more difficult because of the presence of a moving tilt valve. The KIVA series codes developed by Los Alamos National Lab are widely used in 3-D transient numerical simulation of engine. The calculation precision increases gradually. Lebrere and Dillies (1996) calculated the flow in engine using a Reynolds stress model in KIVA-II code. Hessel (1993) employed the snapper technique to treat the moving vertical valve of diesel engines. Kang *et al*.(1995) analyzed the flow in the helical intake port and in the cylinder. Luo *et al*.(2003) dealt with the moving inclined valve by using the re-meshing method. All of them researched just one or two of the four strokes and they researched only the flow in the intake or exhaust manifold. Their researches indicated that these strokes interacted with each other and had their own characteristics respectively. Arias *et al*.(2000) simulated gas exchange process using 1-D model in intake and exhaust processes and 3-D model in other processes. But in fact, the gas flow in an engine is three-dimensional and transient and the tumble and swirl create and vary with piston movement. In order to properly interpret

the results in various simulations, 3-D transient simulation of a complete engine cycle should be carried out. But it is very difficult in practice, mainly because all models (turbulence, injection, combustion, heat transfer) have their own hypotheses in various CFD codes whose numerical scheme precision may sometimes lead to large numerical discrepancies, even wrong results.

In this work, a body-fitted mesh of the whole gas flow field in a four-stroke motorcycle engine was built. An intake valve and exhaust valve model in which each valve can move independently but did not interference with each other was constructed. Three-dimensional transient numerical simulation for four strokes (intake, compression, expand, exhaust) of a motorcycle engine was done with a modified version of KIVA-3 code (Amsden, 1993). The results indicated that the model had higher calculation precision and better future application than other injection and combustion models.

NUMERICAL ANALYTIC MODEL

Governing equations

The governing equations of gas flow consist of mass, momentum and energy conservation equations, turbulence equations, gas state relation equations. The turbulence model is the modified *k*-*ε* turbulence model (Hong and Tang, 1998). The equations are summarized below:

Continuity:

$$\frac{\partial \rho}{\partial t}+\nabla\cdot(\rho \boldsymbol{U})=0 \tag{1}$$

Momentum:

$$\frac{\partial(\rho \boldsymbol{U})}{\partial t}+\nabla\cdot\left(\rho \boldsymbol{U}\boldsymbol{U}\right)=-\nabla P-\nabla\left(\frac{2}{3}\rho k\right)+\nabla\cdot\boldsymbol{\sigma}+\rho g \tag{2}$$

$$\boldsymbol{\sigma}=\mu\left[\nabla \boldsymbol{U}+(\nabla \boldsymbol{U})^{\mathrm{T}}\right]+\lambda\nabla\cdot \boldsymbol{U}I \tag{3}$$

Energy:

$$\frac{\partial(\rho I)}{\partial t}+\nabla\cdot(\rho \boldsymbol{U}I)=-P\nabla\cdot \boldsymbol{U}-\nabla\cdot \boldsymbol{J}+\rho\varepsilon \tag{4}$$

$$\boldsymbol{J}=-K\nabla T-\rho D\sum_m h_m\nabla\left(\frac{\rho_m}{\rho}\right) \tag{5}$$

Turbulence model:

k equation:

$$\frac{\partial(\rho k)}{\partial t}+\nabla\cdot\left(\rho \boldsymbol{U}k\right)=-\frac{2}{3}\rho k\nabla\cdot \boldsymbol{U}+\boldsymbol{\sigma}:\nabla \boldsymbol{U}+\nabla\cdot\left[\left(\frac{\mu}{\mathrm{Pr}_k}\right)\nabla k\right]-\rho\varepsilon \tag{6}$$

ε equation:

$$\frac{\partial(\rho\varepsilon)}{\partial t}+\nabla\cdot(\rho \boldsymbol{U}\varepsilon)=-\left(2c_{\varepsilon_1}/3-c_{\varepsilon_3}\right)\rho\varepsilon\nabla\cdot \boldsymbol{U}+\nabla\cdot\left[\left(\frac{\mu}{\mathrm{Pr}_\varepsilon}\right)\nabla\varepsilon\right]+\frac{\varepsilon}{k}[c_{\varepsilon_1}\boldsymbol{\sigma}:\nabla \boldsymbol{U}-c_{\varepsilon_2}\rho\varepsilon] \tag{7}$$

The quantities c_{ε_1}, c_{ε_2}, c_{ε_3}, Pr_k and Pr_ε are constants whose values are determined from experiments and some theoretical considerations, a feature that establishes certain universality. Standard values of these constants are often used in engine calculations given in below:

$$c_{\varepsilon_1}=1.44,\ c_{\varepsilon_2}=1.92,\ c_{\varepsilon_3}=-1.0,\ \mathrm{Pr}_k=1.0,\ \mathrm{Pr}_\varepsilon=1.3 \tag{8}$$

These equations were solved by the arbitrary Lagrangian-Eulerian (ALE) method that was initially described by Hirt *et al.*(1974). In calculation, the mesh is made up of arbitrary hexahedrons and a cycle or a time step is performed in three phases named A, B and C. Phases A and B together constitute a Lagrangian calculation in which computational cells move with the fluid and convective terms are not considered. Phase A is a calculation of diffusion terms and source terms. In phase B, the new pressure is calculated implicitly. Phase C is Eulerian calculation in which the flow field is frozen and rezoned or remapped onto a new computational mesh and all the convective terms are calculated explicitly. In phase C, the convective terms are discretized by quasi-second-order upwind (QSOU) scheme (Amsden *et al.*, 1989).

Grid generation and computation

The geometry used in this study is the exact geometry of a motorcycle gasoline engine. The combustion chamber is semi-spherical. The engine specifications are: Bore: 50.0 mm; Stroke: 49.5 mm; Speed: 4500 r/min; Displacement volume: 997 cm^3; Intake valve opening: 0° CA after TDC; Intake valve closure: 20° CA after BDC; Exhaust valve opening: 30° CA before BDC; Exhaust valve closure: 2.5° CA before TDC. Fig.1 shows that the computational domain includes intake port, exhaust port, intake valve, exhaust valve and cylinder. The CAD data were taken from Pro/Engineer software to ICEM CFD-HEXA through the International Graphics Exchange Specification (IGES) format. ICEM CFD-HEXA is a grid generation program used to generate a block structured hexahedron grid and to set up boundary conditions for moving valves. As the flow field of motorcycle engine is extremely complex and each valve lift is comparatively short, the mesh generated by ICEM CFD-HEXA directly contains dozens of reversion cells that work improperly for a KIVA-3 input. In order to eliminate these reversion cells, an external program is written to set up proper input file for KIVA-3. In CAD model, neither the intake valve nor exhaust valve locates at its lowest position (BDC, bottom dead center) or its highest position (TDC, top dead center), which makes it easy to build mesh in ICEM CFD-HEXA. A typical computational mesh used in the present study is shown in Fig.2. Total number of computational cells was about 36832 with a typical cell size of 1.7×1.8×1.8 mm^3 and total number of surfaces was about 289. Typical CPU time involved in the simulation of complete gas exchange process was about 29 h on an Intel P4 2.4 G C PC.

Before iteration calculation, a subroutine program was added into KIVA-3 code to adjust the intake valve lift and exhaust valve lift in accordance with the initial crank angle. Dynamic grid generation was accomplished by the re-meshing method and the snapper technique. In the re-meshing method, grids are generated by elliptic grid generation approach. The snapper technique was described by Amsden (1993). When the valve (intake or exhaust) is above the piston TDC plane, the computational domain above the piston TDC plane is divided into several small domains; the dynamic grid of each domain induced by valve movement is generated by the re-meshing method at each time step and then these grids are patched together. The dynamic grids of the computational domain below the piston TDC plane induced by piston movement are generated by the snapper technique. When valve (intake or exhaust) penetrates the piston TDC plane, the grids in the cylinder are first generated according to the snapper tech-

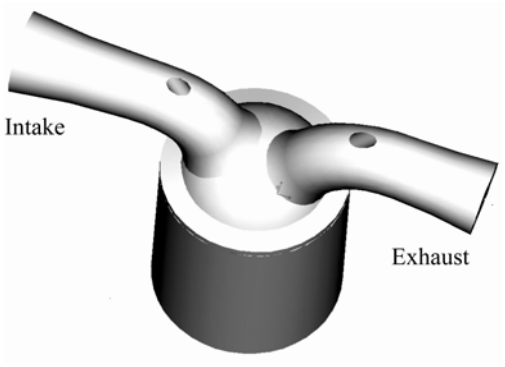

Fig.1 CAD model of computational domain

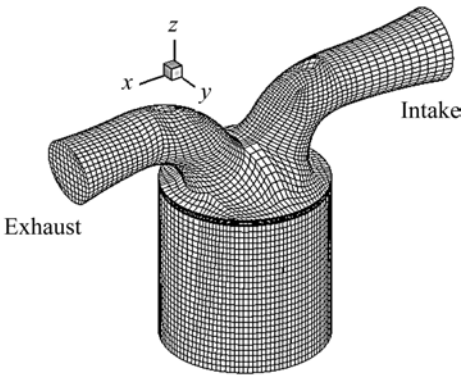

(a)

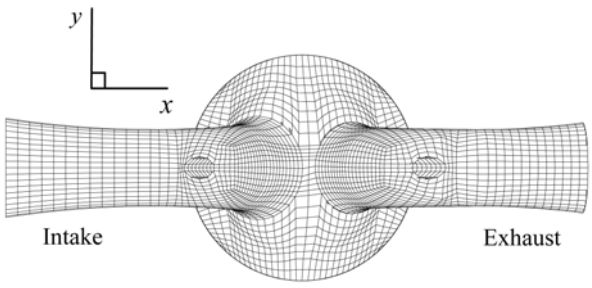

(b)

Fig.2 Computational mesh of motorcycle engine
(a) Perspective view; (b) Top view

nique, then the domain (including the domain above the piston TDC plane and a portion of the cylinder) whose distance away from the piston plane exceeds three layer grids is divided into several small domains, whose dynamic grid is generated by the re-meshing method at each time step and then these new grids are patched together.

During valve high lift, the grids between two valve heads distort and become larger than their initial structure. Some of them may become non-convex, even inversion cells, which will lead to calculation termination. To avoid this case, the exhaust valve head is modified and the intake valve keeps its shape when the intake valve moves down and vice versa.

Initial and boundary conditions

The calculations start at the intake valve opening (IVO, at 0° ATDC, after top dead center) and end at 720° ATDC which is 2.5° CA before the exhaust valve closure. In this study, as the overlap angle which is the timespan when the intake valve and the exhaust valve open simultaneously is very short, only 2.5° CA, this situation should be ignored in calculation. Initially, gas in the computational domain is assumed to be quiescent and its temperature and pressure are assumed to be homogeneous and equal to 360.0 K and 1.1491×10^5 Pa respectively. The computational gas is assumed to be fresh air. The initial value of the turbulent kinetic energy k is assumed to be spatially uniform and is set equal to 10% of the kinetic energy of the mean piston speed kinetic energy. The boundary conditions at inlet and outlet are pressure boundaries. The pressure and temperature at inlet are 0.85×10^5 Pa and 300.0 K respectively. Their values at outlet are kept constant at atmospheric pressure and 300.0 K respectively.

RESULTS AND DISCUSSION

Velocity fields

In order to investigate the velocity flow during the gas exchange process, two sets of center tumble planes were sliced. One was the xz plane (y was zero), the other was the plane normal to the xz plane, that was the yz plane (x was zero).

Fig.3 shows the velocity fields in the xz-plane at different crank angles. Fig.4a shows the intake valve lift profile. Before 10° ATDC, there was some backflow into the intake port as the gas pressure in the cylinder was higher than the intake port pressure. Luo *et al*.(2003) described the backflow in detail. During the first part of the intake process, there were high velocity gradients near the intake valve head and two valve flow jets were visible. There were two small counter-rotating vortexes around the jets. The left one could be seen clearly, but the right one could not be seen clearly because the vortex was confined by the narrow space between two valve heads. This was proved on another xz-plane (y=−0.65) at 20° ATDC, where the right vortex can be clearly visible, as shown in Fig.5. As the piston moved down and the intake valve lift became larger gradually, the two eddies were more evident and strong, with their cores moving downward and rightward little by little. The left eddy was stronger than the right eddy until around 80° ATDC when the two eddies' intensity and displacement almost reached their maximum value simultaneously because of the effect of piston velocity and the maximum lift of the intake valve. After 100° ATDC, the intensity of the left eddy became weaker, its core moved upward and leftward. But the position of the right eddy fluctuated until 160° ATDC, and then its core moved down. Its decay rate was less than that of the left eddy and it was stronger than the left eddy. By the end of the intake process, the right eddy developed large scale tumbling motion and dominated the flow structure, and the other eddy disappeared.

As shown in Fig.3b, in the early part of the compression process, only one eddy exists and the two valve flow jets disappeared with the closing of the intake valve. When the piston moved up, the eddy deformed and split into several small vortexes, but it was still a large scale tumbling motion and its core moved up. At 300° ATDC, the flow developed into a pair of counter rotating vortexes again, with the right vortex being much stronger and larger than the left vortex. The two vortexes existed as strong vertexes until the end of the compression process. In the expansion process, the vortexes rapid became weaker and disappeared at about 400° ATDC. At 510° ATDC, the exhaust valve opened. Fig.4b shows the exhaust valve lift profile. As shown in Fig.3b, the pressure in the exhaust pipe was higher than the pressure inside the cylinder because of the small lift

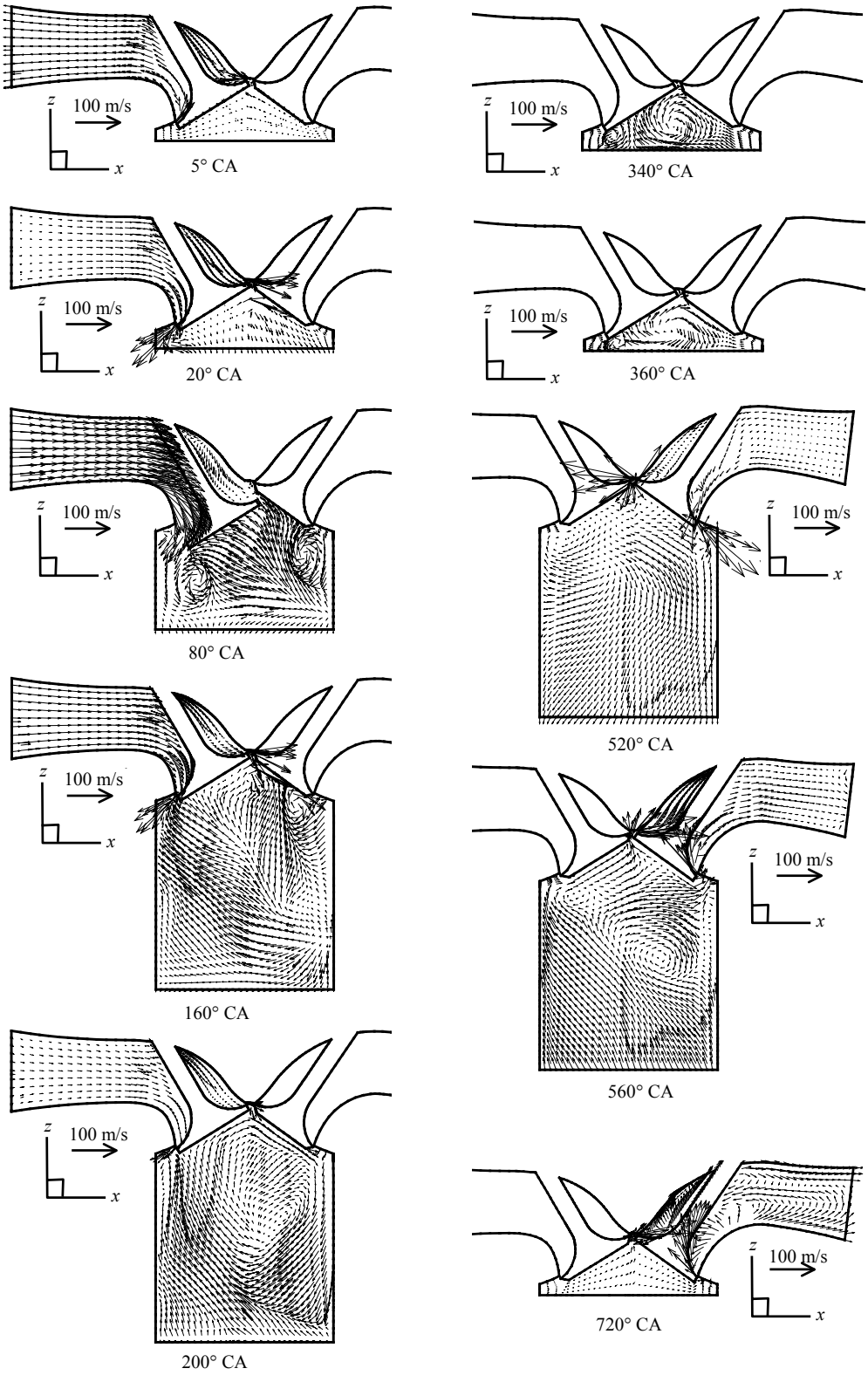

Fig.3 Velocity field on *xz*-plane. (a) Intake process; (b) Compression, expansion and exhaust processes

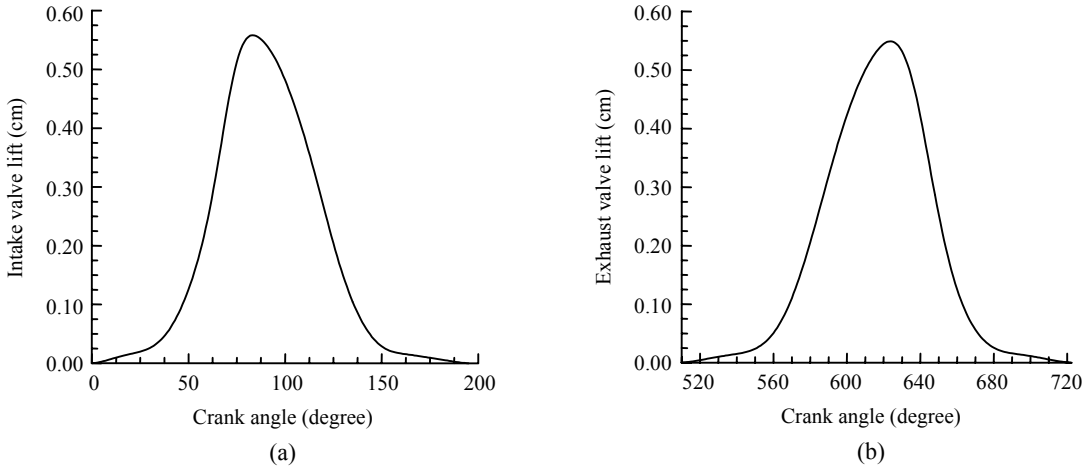

Fig.4 Intake (a) and exhaust (b) valve lift profile

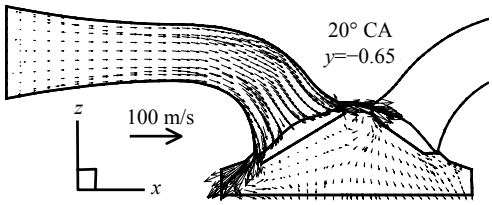

Fig.5 *xz*-plane slice (*y*=−0.65)

of the exhaust valve and the piston is movement towards bottom dead center, which leads to the introduction of two valve jets into the combustion chamber. After 540° ATDC, this situation reversed. At about 560° ATDC, there were two eddies in cylinder, one much larger than the other, with both having the same rotational direction. The duration of this situation was short, the crank angle was approximately 25°. The velocity gradient near the exhaust valve head decreased gradually till the exhaust valve reached its BDC (620° ATDC). In the later part of the exhaust process, the pressure in the exhaust pipe was less than that of the exhaust port with the result that there was backflow in the exhaust port.

Fig.6 shows the crank angle evolution of the flow field in the *yz*-plane. The flow was characterized by two symmetrical, counter-rotating tumbling vortexes growing in size as the piston moved down and were strongest around 90° ATDC. The distance between the two vortexes' cores was relatively large. After that time, the distance decreased gradually and the structures of the two eddies deformed. At 180° ATDC, the counter-rotating eddies became weaker and there were new eddies at the bottom of cylinder. There were around 5~6 not very strong eddies in the full flow field after the intake valve closed. Around the mid stroke of the compression process (270° ATDC), only two eddies, right one being stronger, were still evident. The above flow pattern lasted until the end of the compression process. At 360° ATDC, the right eddy filled 80% of the combustion chamber. In the expansion process, all eddies became weaker and almost disappeared and except for velocity, the flow pattern trended to be identical. In the early part of the exhaust process, two new counter-rotating eddies were formed under the cover and another eddy was formed in the cylinder. But they only lasted a short time due to the increase of the exhaust valve lift.

Mean pressure and tumble ratio

Fig.7 on the variation of the simulated and measured in-cylinder mean pressure data with respect to the crank angle shows reasonable agreement between measured and computed average pressures. The measured average pressure fluctuated at low level in the intake and exhaust strokes, with its value being almost identical with that of the experiment. After 300° ATDC, the average pressure increased rapidly. At the end of the compression stroke, the in-cylinder mean pressure reached a peak of 1.39 MPa, and but was lower than the measured value of 1.59 MPa.

Tumble ratios were calculated to determine the rotational air motion in the cylinder. R_{tx} is tumble ratio

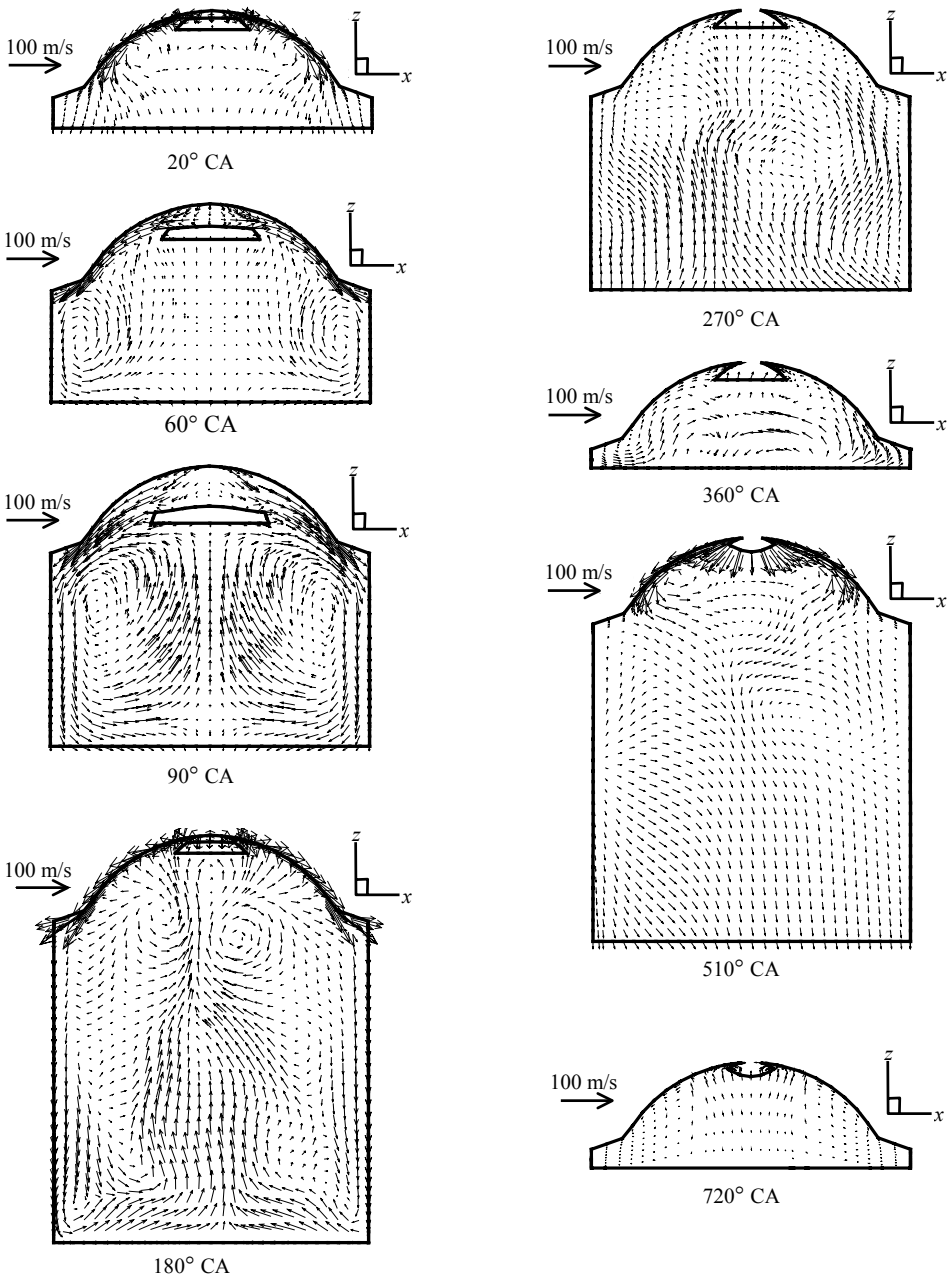

Fig.6 Velocity fields on the *yz*-plane

around the *x*-axis and R_{ty} is tumble ratio around the *y*-axis (Haworth *et al*., 1990; Luo *et al*., 2003).

Fig.8 is the plots of tumble ratios R_{ty} and R_{tx} vs CA. R_{ty} was generally negative in the full cycle. Its absolute value increased rapidly up to 60° ATDC and rapidly decreased to 110° ATDC. This pattern was due to the influence of the strong intake flow in the early part of the intake process and to the rapid increase of piston downward velocity. Interaction of the two counter-rotating eddies was also a causative factor. From 110° ATDC to 150° ATDC, the absolute value increased again, but its gradient was comparatively small. In the compression stroke, R_{ty} decayed rather slowly and almost completely at 360° ATDC. R_{ty} was almost equal to zero in the whole expansion stroke until the exhaust valve opened. R_{ty} increased again in the joint action of piston movement and opening of the exhaust valve and varied

several times. The tumble ratio in the *yz*-plane, R_{tx}, was approximately zero due to the symmetric structure of eddies during the full cycle.

Turbulence intensity

In the calculation, turbulence intensity was determined as follows from the turbulence energy k on the assumption of isotropic turbulence:

$$u'=\sqrt{2k/3} \tag{9}$$

Fig.9 shows the variation of mass-averaged turbulence intensity in the engine cylinder during the intake and compression strokes. The early turbulence intensity fluctuation is due to the sudden opening of the intake valve and closing of the exhaust valve. Before 60° ATDC, the turbulence intensity increased rapidly and reached maximum of about 1.57 m/s in the middle of the intake stroke. During the compression stroke, the turbulence intensity decreased because of the absence of an active mechanism for generating turbulence kinetic energy.

Volumetric efficiency and mass

The volumetric efficiency η_v and gas mass in the engine cylinder were plotted in Fig.10.

In the early part of the intake process, the volumetric efficiency η_v decreased rapidly due to the backflow and the movement of piston. With the intake valve lift becoming larger gradually, η_v increased also. At about BDC of the intake valve, η_v reached its maximum of 0.7, and then decreased till piston BDC. The value of η_v was 0.64 when the intake valve closed.

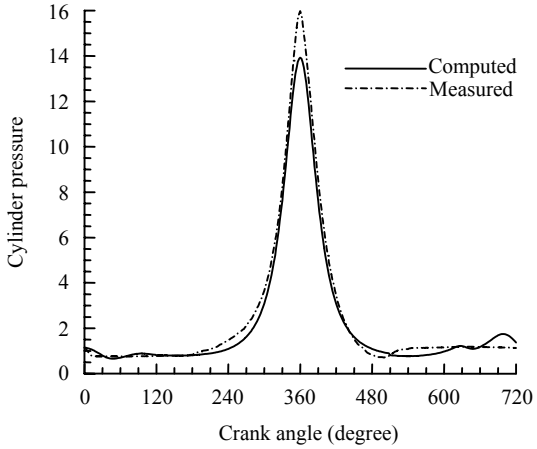

Fig.7 Comparison of measured and computed average pressure

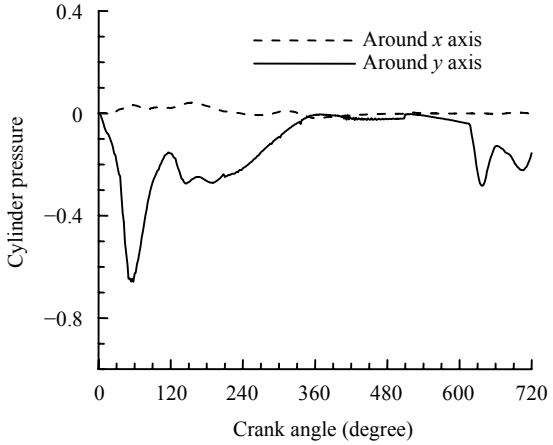

Fig.8 Tumble ratios around *x*-axis and *y*-axis

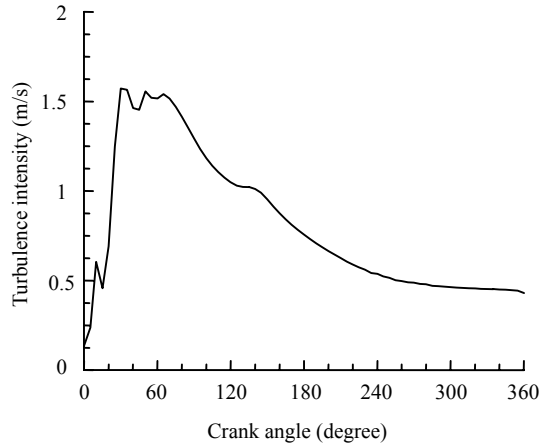

Fig.9 Mass-averaged turbulence intensity

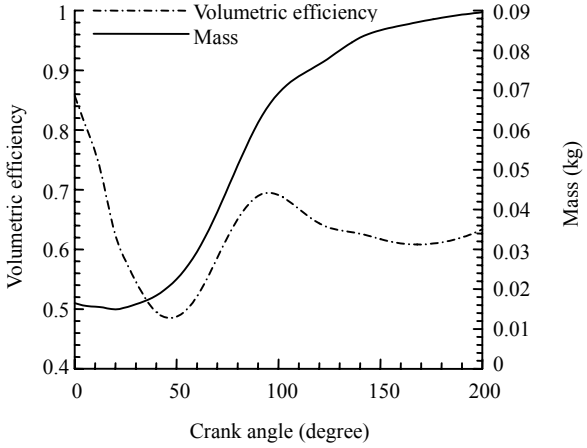

Fig.10 Volumetric efficiency and mass

The gas mass decreased prematurely in the early part of the intake process, and then increased its value to 0.09 kg when the intake valve closed.

CONCLUSION

Three-dimensional numerical simulation was used for studying gas exchange in a four-stroke motorcycle engine under motored condition. A combination of the re-meshing method and the snapper technique can be used to move the intake valve and exhaust valve smoothly. The simulation results revealed detailed information on the flow field. The main gas flow structure is comprised of two counter-rotating eddies. The computed pressure agreeing well with measured pressure under motored condition shows that simulation of gas exchange can be regarded as a good theoretical basis for future work on fuel injection and combustion.

References

Amsden, A.A., O'Rourke, P.J., Butler, T.D., 1989. KIVA-II: A Computer Program for Chemically Reactive Flows with Sprays. Los Alamos National Laboratory Report, No. LA-11560-MS.

Amsden, A.A., 1993. KIVA-3: A KIVA Program with Block-structured Mesh for Complex Geometries. Los Alamos National Laboratory Report, No. LA-12503-MS.

Arias, J.R., Moreno, E., Navarro, E., Varela, E., 2000. Using 1-D and 3-D Models for the Simulation of Gas Exchange Process. SAE Technical Paper Series, No. 2000-01-0658.

Floch, A., Frank, J.V., Ahmed, A., 1995. Comparison of the Effects of Intake-generated Swirl and Tumble on Turbulence Characteristics in 4-valve Engine. SAE, No. 952457.

Gosam, A.D., 1999. State of art of multi-dimensional modeling of engine reactive flows. *Oil & Gas Science and Technology*, **54**(2):149-159.

Haworth, D., Sherif, H., Huebler, M., Chang, S., 1990. Multi-dimensional Port and Cylinder Flow Calculations for Two- and for Valve-per-cylinder Engines: Influence of Intake Configuration on Flow Structure. SAE, No. 900257.

Hessel, R.P., 1993. Numerical Simulation of Valve Intake Port and In-cylinder Flows Using KIVA-3. Ph.D Thesis, University of Wisconsin, US.

Hirt, C.W., Amsden, A.A., Cook, J.L., 1974. An arbitrary Lagrangian-Eulerian computing method for all flow speeds. *J. Comp. Phys.*, **14**:227-243.

Hong, C.W., Tang, S.D., 1998. Direct Measurement and computational analysis of turbulence length scales of a motored engine. *Experiment Thermal and Fluid Science*, **16**:277-285

Johan, Z., Moraes, A.C.M., Buell, J.C., Ferencz, R.M., 2001. In-cylinder cold flow simulation using a finite element method. *Comput. Methods Appl. Mech. Engrg.*, **190**: 3069-3080.

Kang, Y.H., Chang R.C., Jong, G.K., 1995. Flow Analysis of the Helical Intake Port and of a Direct Injection Diesel Engine. SAE, No. 952069.

Kim, Y.J., Lee, S.H., Cho, N.H., 1999. Effect of Air Motion on Fuel Spray Characteristics in a Gasoline Direct Injection Engine. SAE Technical Paper Series, No. 1999-01-0177.

Lebrere, L., Dillies, B., 1996. Engine Flow Calculation Using a Reynolds Stress Model in the KIVA-2 Code. SAE, No. 960636.

Luo, M.J., Chen, G.H., Ma, Y.H., 2003. Three dimensional transient numerical simulation for intake process in the engine intake port-valve-cylinder system. *Journal of Zhejiang University SCIENCE*, **4**(3):309-316.

Zhao, F., Lai, M.C., Harrington, D.L., 1999. Automotive spark-ignited direct-injection gasoline engines. *Progress in Energy and Combustion Science*, **25**:437-562.